

A spectral study of the mid-latitude sporadic E layer characteristic oscillations comparable to those of the tidal and the planetary waves

A. Pignalberi ^a, M. Pezzopane ^{b,*}, E. Zuccheretti ^b

^a Dipartimento di Fisica, Università di Roma "La Sapienza", 00185 Rome, Italy

^b Istituto Nazionale di Geofisica e Vulcanologia, 00143 Rome, Italy

ARTICLE INFO

Article history:

Received 18 April 2014

Received in revised form

7 October 2014

Accepted 29 October 2014

Available online 7 November 2014

Keywords:

Sporadic E layer

Tidal waves

Planetary waves

Wavelet analysis

ABSTRACT

In this paper different spectral analyses are employed to investigate the tidal and planetary wave periodicities imprinted in the following two main characteristics of the sporadic E (Es) layer: the top frequency (ftEs) and the lowest virtual height (h'Es). The study is based on ionograms recorded during the summertime of 2013, and precisely in June, July, August and September, by the Advanced Ionospheric Sounder by Istituto Nazionale di Geofisica e Vulcanologia (AIS-INGV) ionosondes installed at Rome (41.8°N, 12.5°E) and Gibilmanna (37.9°N, 14.0°E), Italy. It was confirmed that the diurnal and semidiurnal atmospheric tides play a fundamental role in the formation of the mid-latitude Es layers, acting through their vertical wind-shear forcing of the long-living metallic ions in the lower thermosphere, and at the same time it was found that the planetary atmospheric waves might affect the Es layers acting through their horizontal wind-shear forcing with periods close to the normal Rossby modes, that is 2, 5, 10 and 16 days. The wavelet analysis shows also that the ftEs and h'Es tidal oscillations undergo a strong amplitude modulation with periods of several days and with important differences between the two parameters. This amplitude modulation, characterizing markedly the first thirty days of the ftEs spectrogram, suggests that Es layers are affected indirectly by planetary waves through their nonlinear interaction with the atmospheric tides at lower altitudes. This study wants to be a continuation of the [Haldoupis et al. \(2004\)](#) work in order to verify their results for the foEs characteristic and on the other hand to extend the study also to the h'Es characteristic not yet shown so far. Anyhow, the study confirms that ionosonde data, especially those registered in summertime, represent a powerful tool for studying tidal and planetary waves properties and their climatology in the mesosphere–low-thermosphere region.

© 2014 Elsevier Ltd. All rights reserved.

1. Introduction

The mid-latitude sporadic E (Es) layers, whose characteristics have been studied for many years (see reviews by [Whitehead, 1989](#); [Mathews, 1998](#); [Haldoupis, 2011, 2012](#)), are thin and dense layers of plasma forming mostly in the mesosphere–low-thermosphere (MLT) region between 90 and 130 km, a region characterized by complicated dynamics and nonlinear plasma processes. The Es phenomenon is in fact itself representative of the complex interaction between the neutral atmosphere wave dynamics and the ionosphere which occurs right in this region.

As a proof of the complexity and intricacy of the phenomenon, [Mathews et al. \(1993\)](#) using incoherent scatter radar observations showed that ion layers are almost continuously present in the 80–150 km altitude region above Arecibo, and they identified three

different categories. The first category includes those layers that, due to their highly periodic behavior, are associated with the tidal waves (TWs) and referred to as tidal ion layers (TILs); TILs include the classical intermediate layers, associated with the semidiurnal TW, as well as the lower-lying layers that have been traditionally known as sporadic E layers and are largely controlled by the diurnal TW, although a mix of TWs is often involved, and are convincingly held to be formed via the classical wind-shear mechanism. The second category includes all sporadic layers (layers which are unexpected in location and/or intensity) including sporadic intermediate layers, true sporadic E in the 90–110 km region, and associated sporadic neutral-metal layers; these layers are found in a rich context of related phenomena that includes the TILs, electric-field-induced layers, HF/VHF radar quasi-periodic echoing (QPE) regions, and ion rain as discussed by [Mathews \(1998\)](#), [Mathews et al. \(2001\)](#), and [Otsuka et al. \(2007\)](#); in particular, [Mathews \(1998\)](#) and [Otsuka et al. \(2007\)](#) concluded that the QPEs and ion rain indicate small horizontal scales and found

* Corresponding author.

E-mail address: michael.pezzopane@ingv.it (M. Pezzopane).

considerable other evidence of 10–100 km scale horizontal-structuring of layers suggesting an E/F region electrodynamic coupling, apparently including instability-generated 10–100 km horizontal-scale E fields that are hypothesized to generate true sporadic E and the related complex layer structures (CLS) via horizontal redistribution of ions. The third category includes very low-lying layers that occur down to an altitude of about 82 km which cannot be seen by an ionosonde.

According to the first category, it is believed that the formation of Es relies on vertical wind shears in the neutral horizontal winds with a proper polarity, which can cause, along with the combined action of ion-neutral collisional coupling and geomagnetic Lorentz forcing, the long-lived metallic ions of meteoric origin to move vertically and converge into dense and thin plasma layers localized at the convergence node of the neutral horizontal wind vertical profile. In this process the magnetized electrons simply follow the ions by moving along the field lines to maintain charge neutrality (Rishbeth and Garriott, 1969). This vertical wind-shear mechanism was formulated in the early 60s studies about the Es phenomenon, mostly associated with the atmospheric gravity waves (Whitehead, 1961; Axford, 1963; Chimonas and Axford, 1968). Further studies by Fujitaka and Tohmatsu (1973), Wilkinson et al. (1992), and Szuszczewicz et al. (1995), based on ionosonde data, demonstrated the importance of the TW influence imprinted in the Es characteristics. This influence has been recently investigated by Haldoupis et al. (2006), who proposed a new methodology named height-time-intensity (HTI) to study how the TWs control the Es dynamics.

More recently, it has been recognized also the importance of the planetary waves (PWs), that set up a horizontal wind-shear mechanism causing a plasma accumulation in areas of positive vorticity, as formulated by Shalimov et al. (1999) and Shalimov and Haldoupis (2002), and then verified by the Haldoupis and Pancheva (2002) and Pancheva et al. (2003). Planetary waves are global oscillations of the neutral atmosphere at periods of about 2, 5, 10 and 16 days, also called Rossby normal modes (Holton, 1975; Forbes, 1995); they are mainly of tropospheric origin and can penetrate directly to height slightly above 100 km as it was earlier theoretically proposed by Charney and Drazin (1961) and Dickinson (1968) and recently experimentally verified by Pancheva and Mukhtarov (2000), this penetration being critically dependent on the zonal wind flow intensity.

Haldoupis et al. (2004) found an amplitude modulation of the TW periodicities, with periods of days, characterizing the Es critical frequency of the ordinary wave component (foEs) time series, and they associated this phenomenon to a nonlinear wave interaction between the TWs and the PWs concurrently present at low altitudes. Sauli and Bourdillon (2008) showed the same amplitude modulation affecting the lowest virtual height of the Es trace (h'Es). This mechanism of nonlinear interaction, formulated by Teitelbaum and Vial (1991) and verified in neutral atmospheric winds studies (Beard et al., 1999; Pancheva et al., 2000a, 2000b; Pancheva, 2000; Pancheva and Mukhtarov, 2000), causes the appearance of secondary waves having frequencies that are the sum and difference of the waves frequencies involved in the interaction, according to the Teitelbaum and Vial (1991) theory. It is worth noting that, unlike the TWs, the PWs are not to be necessarily present at the investigated ionospheric region, since their nonlinear modulation may occur in the lower atmospheric region and be transported by the TWs to upper regions, where the PWs might not propagate.

In this paper we show the variability of the oscillations, comparable to those of the TWs and the PWs, imprinted in the time series of the top frequency of the Es layer (ftEs) and h'Es measured during a summertime campaign carried out at two mid-latitude ionospheric stations. These Es layer oscillations are investigated by

means of the Fast Fourier Transform (FFT) and the Windowed Fourier Transform (WFT) amplitude spectra, and by the Continuous Wavelet Transform (CWT) spectrograms. The purpose of the work is to study in detail the tidal amplitude modulation affecting both ftEs and h'Es, and relate it to the Teitelbaum and Vial (1991) theory.

This study comes as a continuation of the Haldoupis et al. (2004) work, as a first step to verify their results for the foEs characteristic, but also to make additional considerations about the h'Es characteristic.

2. Data and methods of analysis

The ionograms used to make the ftEs and h'Es time series employed in this study were recorded during a summertime campaign (4 June–30 September 2013) by the Advanced Ionospheric Sounder-Istituto Nazionale di Geofisica e Vulcanologia (AIS-INGV) ionosondes (Zuccheretti et al., 2003) installed at Rome (Italy, 41.8°N, 12.5°E) and Gibilmanna (Italy, 37.9°N, 14.0°E), with a sounding repetition rate of 5 and 15 min respectively. The corresponding sweeping frequency range was set up from 1 MHz to 16 MHz at both stations, with a frequency resolution of 0.05 MHz; the height range investigated by the AIS-INGV ionosonde is 90–760.5 km with a height resolution of 4.5 km, these two altitude settings being fixed and depending on the architectural features of the ionosonde. The Gibilmanna data were essentially used to assess and validate the significance of the results obtained for Rome.

This study was performed considering summertime ionograms since it is known that Es layer is most pronounced in this period (Haldoupis et al., 2007; Pietrella and Bianchi, 2009). Inspection of ionograms showed the presence of fairly continuous Es layers from early June to late September, which allowed for a reasonably complete time series of the Es characteristics to be obtained. From each ionogram the ftEs expressed in MHz, and the h'Es expressed in km, were manually validated through the graphical user interface of the software *Interpre* (Pezzopane, 2004). It was decided to refer to ftEs and not to foEs because the AIS-INGV ionosonde cannot tag the different modes of propagation, that is the extraordinary (X) and the ordinary (O) ones, and for most of ionograms was practically impossible to distinguish between foEs and the critical frequency (fxEs) of the Es extraordinary mode. The characteristic ftEs is an estimate of the maximum electron density of the Es layer, and it is directly associated to the efficiency of the wind-shear theory; the characteristic h'Es provides information about the location of the Es layer, hence it is the best characteristic for studying the Es diurnal dynamics.

In order to reduce data gaps caused by the absence of the layer, ftEs and h'Es hourly means were considered. In this way there were only few data gaps due mainly to the absence of Es layer, mostly in late August and September. In order to have complete time series, which is a constraint of the wavelet transform algorithm used in our study, the gaps were filled with the corresponding monthly mean values; in this way, two complete ftEs and h'Es time series of 2856 hourly mean values, corresponding to the 119 days of the whole sounding campaign (4 June–30 September 2013), were obtained for Rome and Gibilmanna.

In order to determine the prevailing TW periodicities, the Fast Fourier Transform (FFT) spectral analysis was selected to compute amplitude spectra of the ftEs and h'Es time series, for periodicities from 2 to 36 h. The Windowed Fourier Transform (WFT) spectral analysis was instead selected to point out the PW periodicities from 1.5 to 20 days. This different choice is because the two wave phenomena under investigation have different characteristics; it is known in fact that the TWs influence continuously Es layers with diurnal and semidiurnal periodicities (Haldoupis et al., 2004,

2006), and then can be considered as a stationary phenomenon, while the PWs influence Es layers only for a definite time (typically of a few weeks) with periods similar to those of the normal Rossby modes, and then can be considered as transient phenomena.

In order to study in more detail the TW and PW periodicities imprinted in the Es time series, the Morlet wavelet was also applied (Torrence and Compo, 1998, and references therein); the corresponding wavelet spectrograms are very useful to highlight the dynamic changes in the ftEs and h'Es spectral content, mostly concerning the amplitude modulation suffered by TW periodicities, but also to obtain a temporal characterization of the PWs, which is impossible by using the FFT and WFT methods.

When applying the CWT, FFT and WFT methods, to avoid *edge problems* and *cut problems*, from the ftEs and h'Es time series the corresponding mean value was subtracted (obtaining as a consequence two zero mean time series) and zeros at the beginning and at the end of the time series were added up to reach the nearest multiple of 2 of values (4096 in our case).

3. Spectral analysis of the ftEs and h'Es time series

This section describes the application of the FFT, WFT, and CWT analyses to the ftEs and h'Es Rome and Gibilmanna time series to investigate how these are affected by the TW and PW periodicities.

3.1. Tidal wave periodicities affecting the Es layer: the Rome case

Fig. 1a shows the ftEs hourly mean values recorded at Rome from the 4 June (day 155) to the 30 September (day 273) 2013, which presents a pronounced diurnal variability, with values ranging from about 2 to 15 MHz; the corresponding 72 h running mean (the thick line in Fig. 1a) ranges between 4 and 6 MHz, and is amplitude modulated at a much slower rate, with periods from a few to several days. The amplitude modulation is particularly evident in the first half of the time series (June and July), where the ftEs values are higher, accordingly to the seasonal behavior characterizing the Es layer and recently well explained in terms of the meteoric influx near the summer solstice (Haldoupis et al., 2007).

To identify the ftEs TW periodicities, the FFT amplitude spectrum of the ftEs time series was performed for periods ranging from 2 to 36 h (Fig. 1b). This amplitude spectrum is dominated by two narrow spectral peaks at 12 and 24 h that greatly exceed the 95% level of confidence, and that are reasonably associated to the diurnal and semidiurnal TWs through the vertical wind-shear mechanism. To further investigate this feature, a CWT analysis of the ftEs time series was also performed for periods ranging from 6 to 36 h (Fig. 1c). Also the CWT analysis confirms that the strongest components are mostly around the 12 h and 24 h periods, the latter being the most important, as it was already highlighted by the FFT analysis. Anyway, the CWT spectrogram shows that the amplitudes of the tidal-like periodicities are strongly modulated in time with a period of several days, above all in the first half of the time series, as it was previously seen in Fig. 1a; the theory of Teitelbaum and Vial (1991) suggests that this could be caused by a TW–PW nonlinear interaction, which will be investigated later in more detail.

The same analysis was also performed for the h'Es characteristic. Fig. 2a shows the h'Es hourly mean value time series recorded from the 4 June (day 155) to the 30 September (day 273) 2013, which presents a pronounced diurnal variability, with values ranging from about 94 to 130 km; the corresponding 72 h running mean (the thick line in Fig. 2a) ranges between 102 and 110 km, and alike ftEs is amplitude modulated with periods from a few to several days. However, unlike ftEs, the h'Es amplitude modulation

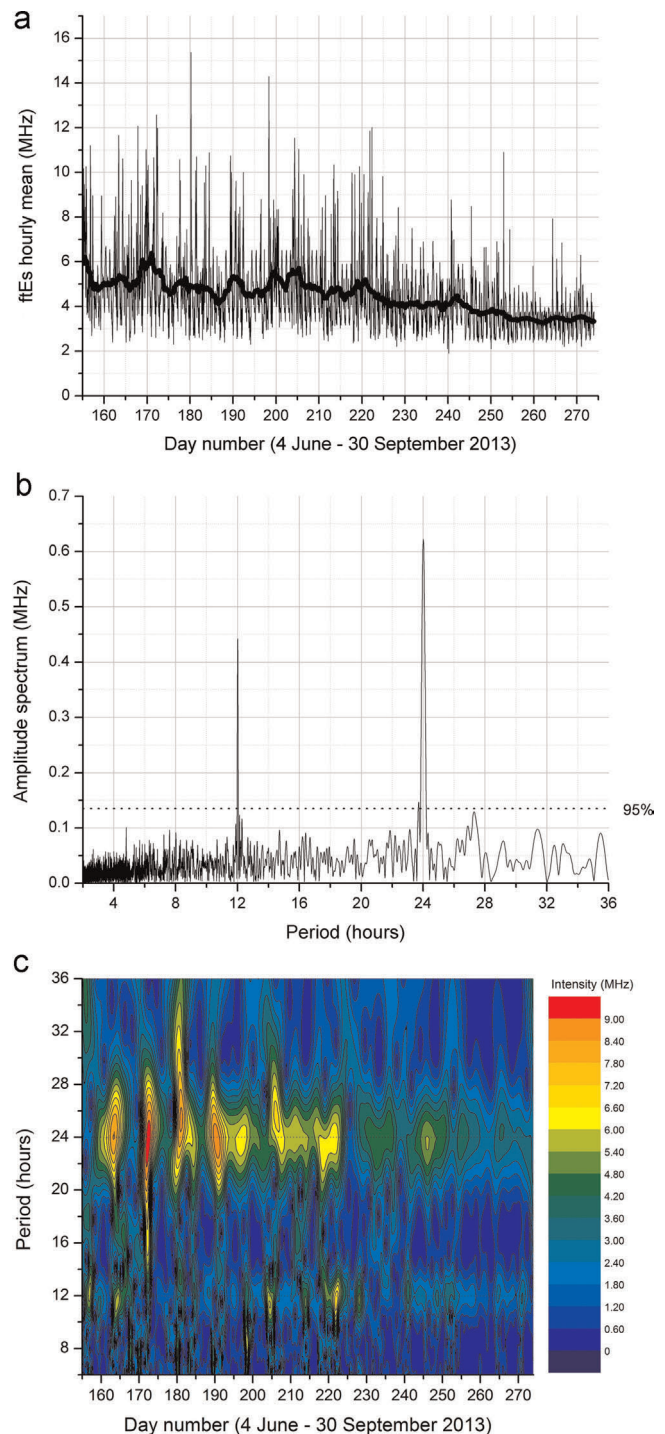


Fig. 1. (a) ftEs hourly mean values recorded at Rome from the 4 June to the 30 September 2013 (the thick line represents the 72 h running mean). (b) FFT amplitude spectrum of the ftEs time series shown in (a) for period ranging from 2 to 36 h (the horizontal dashed line indicates the 95% level of confidence). (c) Wavelet spectrogram of the ftEs time series shown in (a) for periods ranging from 6 to 36 h.

is present throughout the time series, this fact highlighting the different physical meaning distinguishing the two characteristics. Fig. 2b shows the FFT amplitude spectrum of the h'Es time series for periods ranging from 2 to 36 h. Unlike ftEs, the h'Es amplitude spectrum is characterized by several narrow spectral peaks at 6, 8, 12 and 24 h exceeding the 95% level of confidence, that are reasonably associated to the TW periodicities that are sub-harmonics of the solar day; however, also in this case, the 12 h and 24 h peaks are the most intense. Fig. 2c shows the CWT spectrogram of the

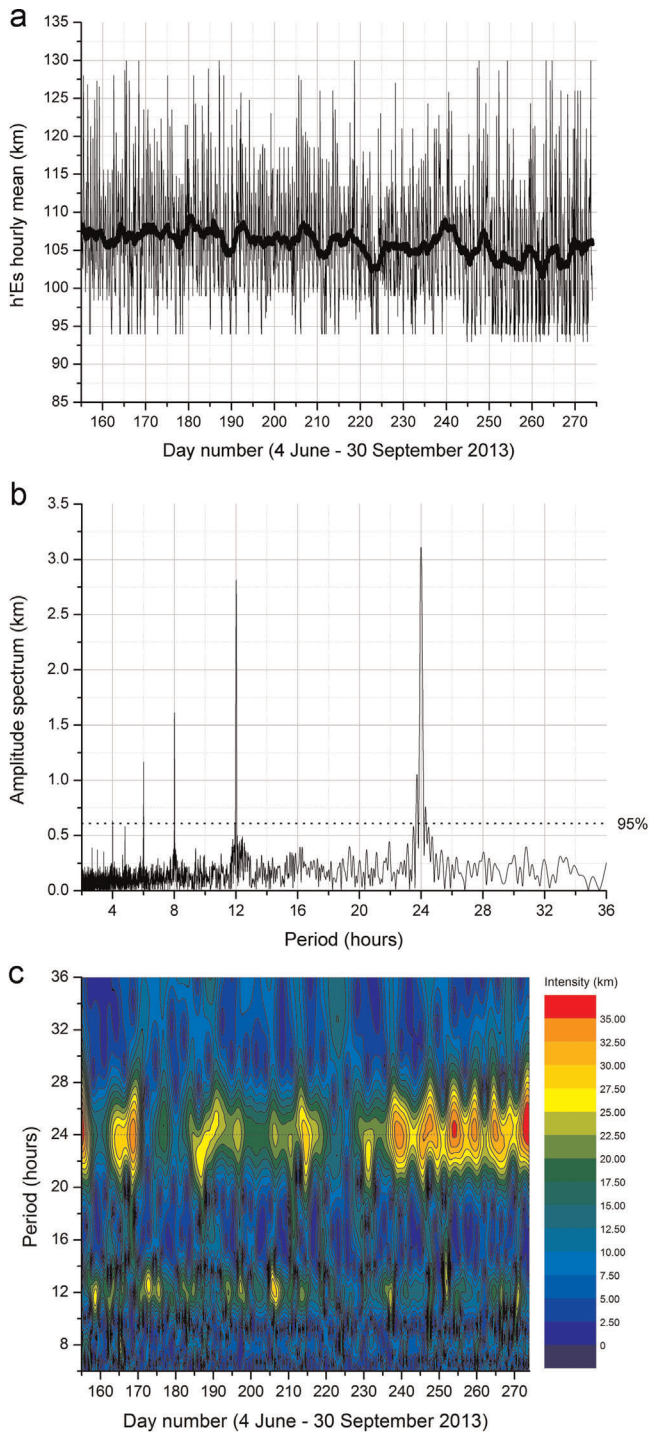


Fig. 2. (a) h'Es hourly mean values recorded at Rome from the 4 June to the 30 September 2013 (the thick line represents the 72 h running mean). (b) FFT amplitude spectrum of the h'Es time series shown in (a) for period ranging from 2 to 36 h (the horizontal dashed line indicates the 95% level of confidence). (c) Wavelet spectrogram of the h'Es time series shown in (a) for periods ranging from 6 to 36 h.

h'Es time series for periods ranging from 6 to 36 h. Alike ftEs, also for h'Es the strongest components are mostly around the 12 h and 24 h periods, the latter being the most important, whereas the other components at 6 and 8 h pointed out by the FFT analysis are much weaker. Also in this case the CWT spectrogram shows that the amplitudes of the tidal-like periodicities are strongly modulated in time with a period of several days.

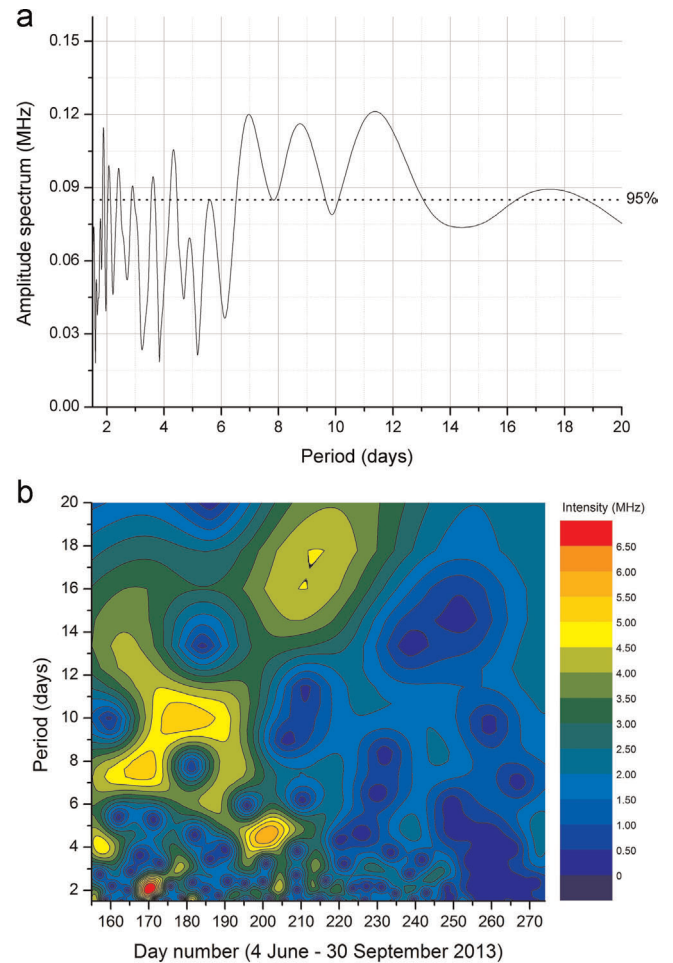


Fig. 3. (a) WFT amplitude spectrum (the horizontal dashed line indicates the 95% level of confidence) and (b) Wavelet spectrogram of the ftEs time series shown in Fig. 1a for periods ranging from 1.5 to 20 days.

3.2. Planetary wave periodicities affecting the Es layer: the Rome case

Fig. 3a shows the WFT amplitude spectrum of the ftEs time series shown in Fig. 1a, for periods ranging from 1.5 to 20 days. This spectrum is characterized by several more or less narrow spectral peaks at about 2, 5, 7, 9, 11 and 17 days exceeding the 95% level of confidence. The peaks with periods ranging from 2 to 5 days are very narrow and this means that they have a low energy content, while the peaks at 7, 9, 11 and 17 days are wide, this implying a high energy content. These spectral peaks are reasonably associated to the PWs through the horizontal wind-shear mechanism proposed by Shalimov et al. (1999) and Shalimov and Haldoupis (2002). To further investigate this feature, a CWT analysis of the ftEs time series was performed for periods ranging from 1.5 to 20 days (Fig. 3b). The corresponding spectrogram shows that the strongest components are mostly around the 2, 4, 5, 7–8, 10 and 17 day periods, that are more or less the normal Rossby modes of the PWs; the differences between the theoretical and experimental periods are due mainly to the fact that we are not analyzing directly the winds in the E region but the effects that there have on Es through the horizontal wind-shear mechanism. As might be expected, the greater the period of the PW, the greater the energy content because the greater the duration of the wave phenomenon, so even though the maximum intensity is associated to the 2 day period around the day 170, the maximum energy content is associated to the 7–11 day periods characterizing

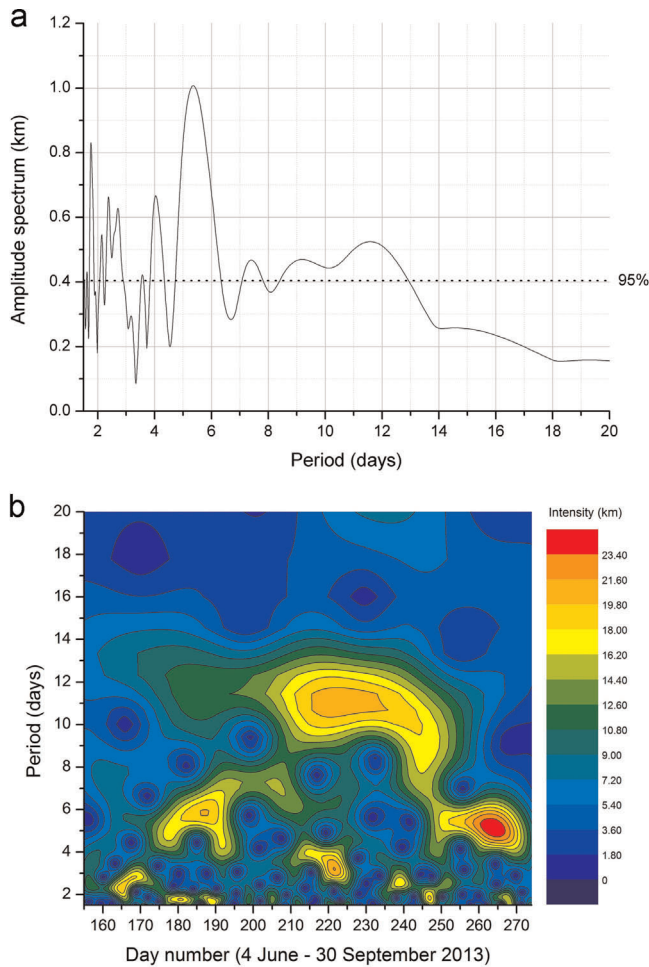


Fig. 4. (a) WFT amplitude spectrum (the horizontal dashed line indicates the 95% level of confidence) and (b) Wavelet spectrogram of the h'Es time series shown in Fig. 2a for periods ranging from 1.5 to 20 days.

the first 30 days of the time series. As it was already seen for the TW periodicities, also for the PW periodicities the results are affected by the seasonal behavior characterizing the Es layer and recently well explained in terms of the meteoric influx near the summer solstice (Haldoupis et al., 2007).

Fig. 4a shows the WFT amplitude spectrum of the h'Es time series shown in Fig. 2a, for periods ranging from 1.5 to 20 days. This amplitude spectrum is characterized by several more or less narrow spectral peaks at about 1.5–2, 2.5, 4, 5–6, 7–8 and 9–12 days exceeding the 95% level of confidence. The peaks with periods between 1.5 and 4 days are very narrow implying a low energy content, while the peaks with periods between 5 and 12 days are wide implying a high energy content. Similarly to the spectral peaks characterizing ftEs, also these peaks are reasonably associated to the PWs through the horizontal wind-shear mechanism; anyway, the most striking feature is that the periods shown by the h'Es WFT analysis are quite different than those shown by the ftEs WFT analysis shown in Fig. 3a. To further investigate this influence, a CWT analysis of the h'Es time series was also performed for periods ranging from 1.5 to 20 days (Fig. 4b). The CWT spectrogram confirms that the strongest components are mostly those with periods of around 1.5–3, 5–6 and 9–12 days. The maximum energy content is associated to the 5–6 and 9–12 day periods located, respectively, in the last 20 days and between the days 210 and 250 of the time series. Overall, alike the TW periodicities, also the h'Es PW periodicities do not present a clear seasonal behavior.

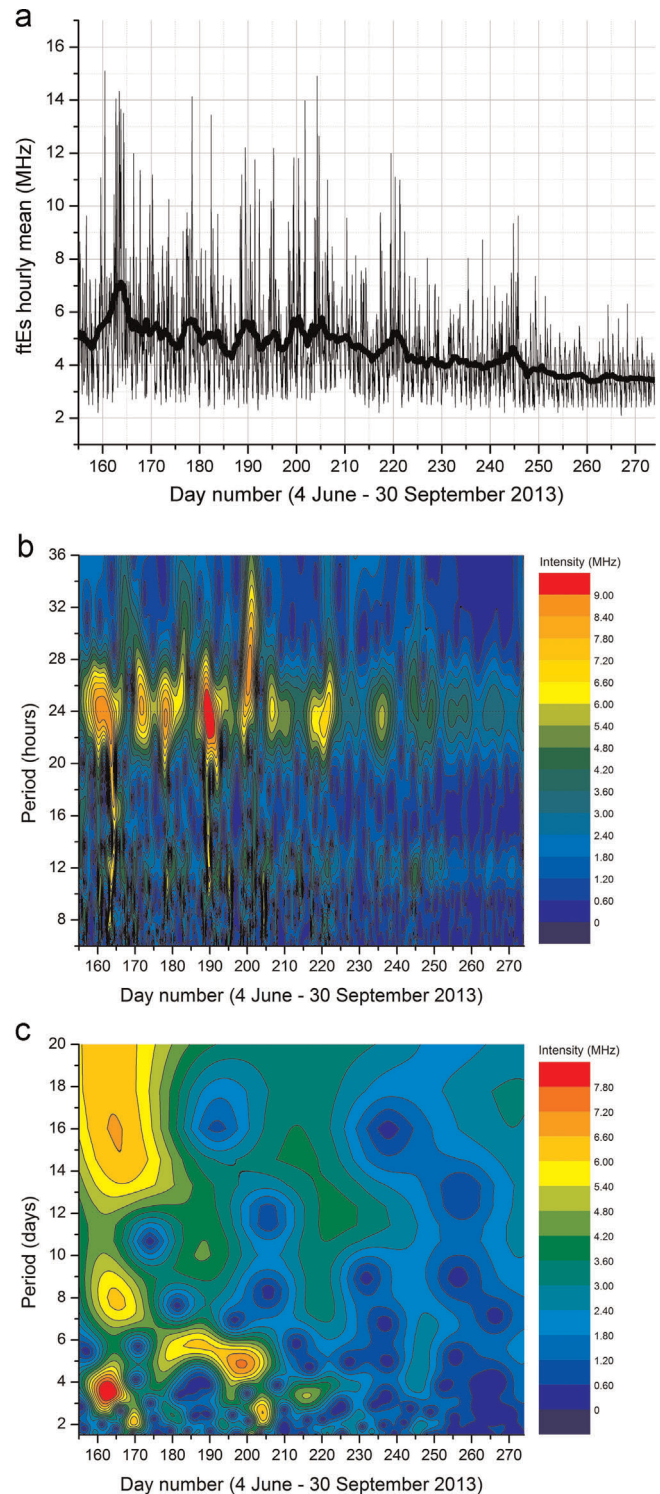


Fig. 5. (a) ftEs hourly mean values recorded at Gibilmanna from the 4 June to the 30 September 2013 (the thick line represents the 72 h running mean). (b) Wavelet spectrogram of the ftEs time series shown in (a) for periods ranging from 6 to 36 h. (c) Wavelet spectrogram of the ftEs time series shown in (a) for periods ranging from 1.5 to 20 days.

3.3. Tidal and planetary wave periodicities affecting the Es layer: the Gibilmanna case

In order to assess and validate the significance of the results obtained for Rome and described in Sections 3.1 and 3.2, the same spectral analyses were carried out on data recorded at Gibilmanna,

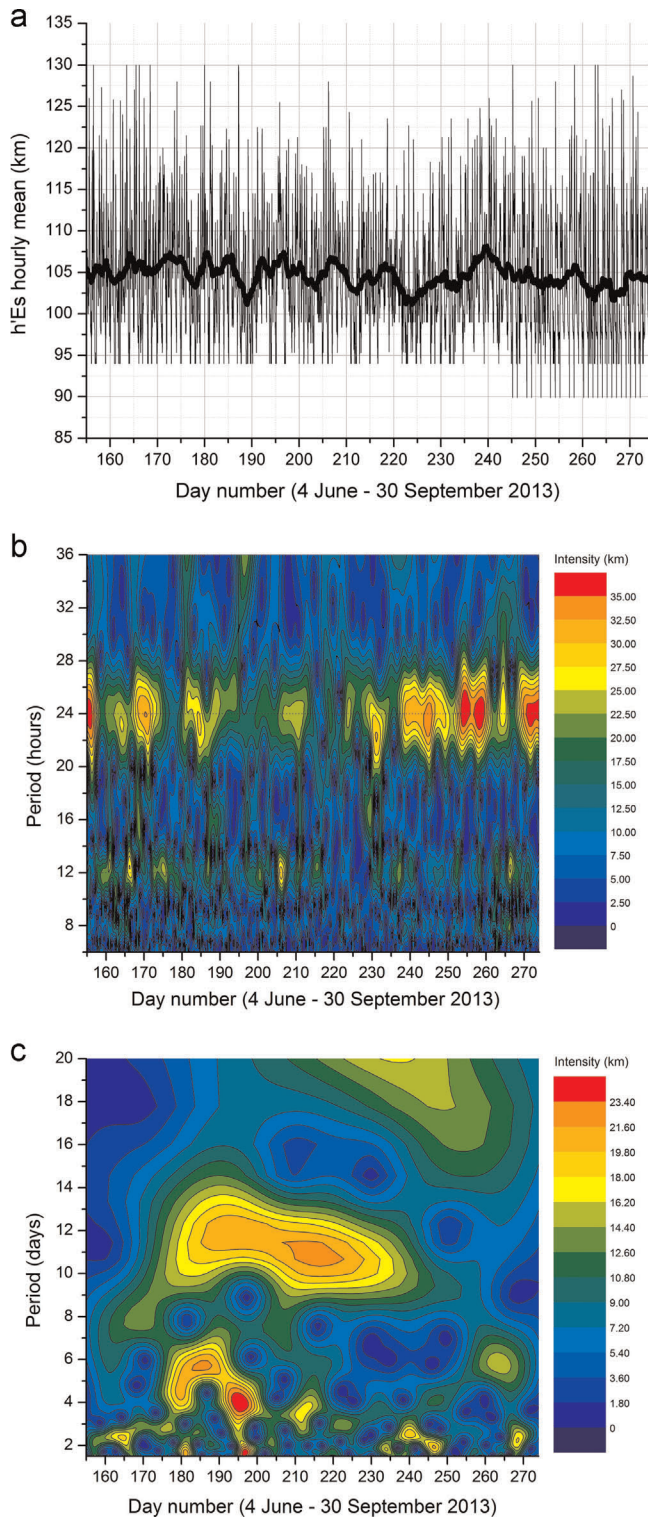


Fig. 6. (a) h'Es hourly mean values recorded at Gibilmanna from the 4 June to the 30 September 2013 (the thick line represents the 72 h running mean). (b) Wavelet spectrogram of the h'Es time series shown in (a) for periods ranging from 6 to 36 h. (c) Wavelet spectrogram of the h'Es time series shown in (a) for periods ranging from 1.5 to 20 days.

which is approximately 450 km far from Rome and differs in latitude by about 4° southward. Fig. 5a shows the ftEs hourly mean values recorded at Gibilmanna from the 4 June (day 155) to the 30 September (day 273) 2013; Fig. 5b and c shows instead the corresponding CWT spectrograms for the TW periodicities and the PW periodicities, respectively. The only difference between the

analyses made on Rome data and on Gibilmanna data is that the sounding repetition rate at Gibilmanna was set to 15 min while at Rome was set to 5 min, which may result in a lower resolution characterizing the Gibilmanna spectra. Anyhow, the Gibilmanna results are in good agreement with the Rome results, mostly for what concerns the TW periodicities (Figs. 1c and 5b), whereas the PW periodicities (Fig. 3b and 5c) show some differences mostly related to an intensification of the higher periods (14–20 days) in the first part of the time series characterizing the Gibilmanna spectrogram.

Fig. 6a shows the h'Es hourly mean values recorded at Gibilmanna from the 4 June (day 155) to the 30 September (day 273) 2013, while Fig. 6b and c shows the corresponding CWT spectrograms for the TW periodicities and the PW periodicities, respectively. The Gibilmanna results are in good agreement with the Rome results both in terms of TW periodicities (Figs. 2c and 6b) and in terms of PW periodicities (Fig. 4b and 6c).

The fairly good correspondence between the Rome and Gibilmanna results suggests that the oscillations embedded in the Rome and Gibilmanna Es data are both realistic and significant. Moreover, the distance between the two sites indicates that these oscillations are caused by large-scale processes, a fact that agrees very well with the notion of TWs and PWs. The small differences characterizing mostly the PW periodicities could be due to the small difference in latitude between the two sites; in fact, the PWs exhibit a pronounced variability in latitude (Pancheva and Mukhtarov, 2011) and the properties of the vertical propagation depend critically on the zonal mean flow (Charney and Drazin, 1961; Dickinson, 1968).

4. TW–PW nonlinear interaction

Figs. 1c and 2c show clearly that the diurnal and semidiurnal TW periodicities imprinted both in ftEs and h'Es are modulated in amplitude with periods of several days. In order to study in more detail how much this phenomenon is due to the nonlinear interaction between the TWs and the PWs, the time series associated to the diurnal and semidiurnal periodicities were extracted and filtered from the corresponding spectrograms shown in Figs. 1c and 2c according to the following steps: (a) the wavelet coefficients with periods from 20 to 28 h, and with periods from 10 to 14 h, were selected; (b) the inverse wavelet transform was applied to these coefficients in order to extract the signals related to the diurnal and semidiurnal periodicities; (c) a low-pass filter was applied to obtain the time series showing the modulation caused by the PWs; and (d) a CWT was then applied again to these filtered time series to find out which PW modes interacted nonlinearly with the diurnal and semidiurnal TW periodicities imprinted in the Es time series. In the following two sections, the corresponding results obtained respectively for the diurnal and the semidiurnal periodicities are described.

4.1. The case of the diurnal tidal periodicity

Fig. 7a shows the signal related to the diurnal TW periodicity characterizing ftEs after applying the aforementioned steps (a) and (b) starting from the spectrogram shown in Fig. 1c. As expected, the signal appears as an AM radio signal, it has a carrier wave with a period of 24 h and a modulating wave with a variable period of many days. Fig. 7b shows instead the ftEs diurnal periodicity time series obtained from the signal shown in Fig. 7a after straightening and low-filtering it, and Fig. 7c shows the corresponding wavelet spectrogram for PW periods. Fig. 7c shows that the most important feature is associated to a large spectral peak with a period ranging from about 7 to 11 days centered around the 9 day

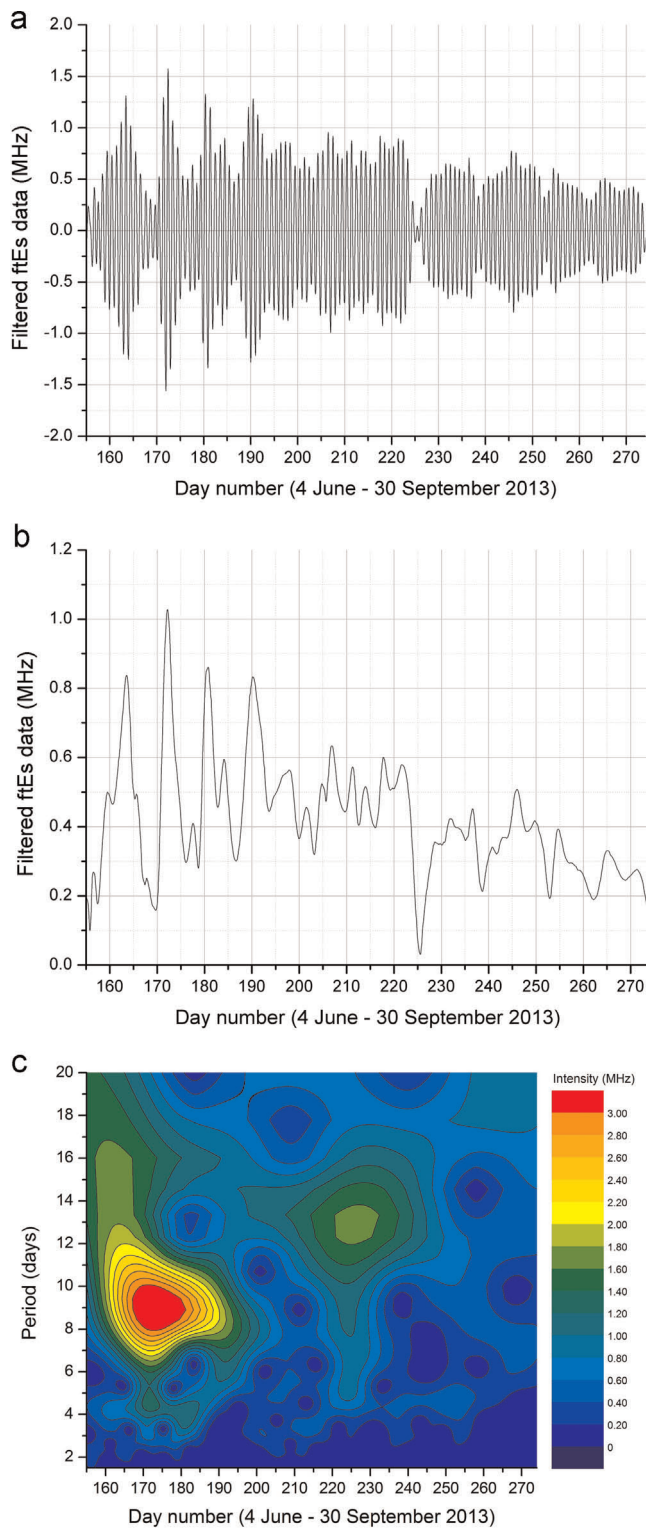


Fig. 7. (a) The ftEs signal related to the diurnal periodicity extracted from the spectrogram shown in Fig. 1c. (b) The ftEs diurnal periodicity time series obtained from the signal shown in (a) after straightening and low-filtering it. (c) The wavelet spectrogram of the time series shown in (b) for periods ranging from 1.5 to 20 days.

periods, tagging the first 30 days of the time series (4 June–4 July 2013); in the same sector minor peaks for periods of about 4 and 14–18 days are also present, while between the days 210 and 240 a less important spectral peak for periods ranging from 10 to 16 days is present.

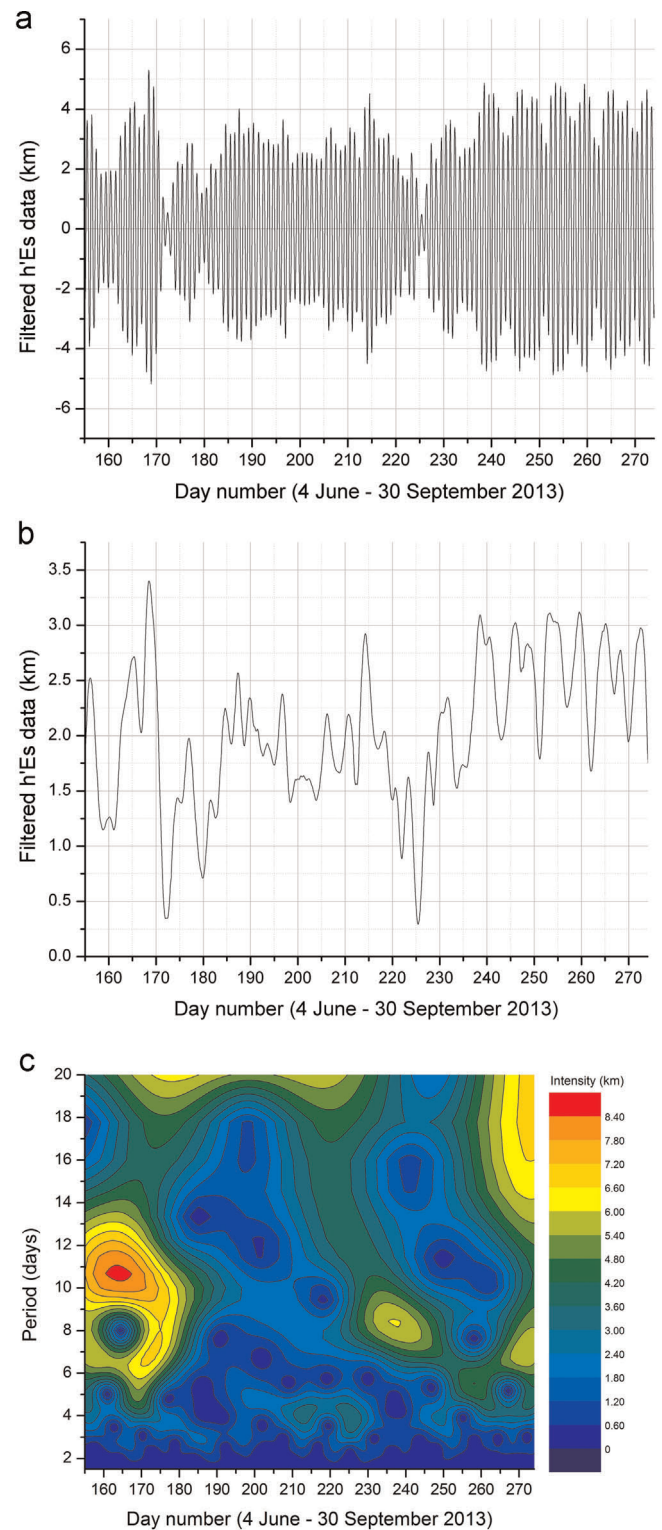


Fig. 8. (a) The h'Es signal related to the diurnal periodicity extracted from the spectrogram shown in Fig. 2c. (b) The h'Es diurnal periodicity time series obtained from the signal shown in (a) after straightening and low-filtering it. (c) The wavelet spectrogram of the time series shown in (b) for periods ranging from 1.5 to 20 days.

Fig. 8 is the same as Fig. 7 but for h'Es. The wavelet spectrogram of Fig. 8c shows that the first part of the time series is pretty similar to that found for ftEs (Fig. 7c) with the most important peak centered at a period of about 11 days, while other minor peaks are localized at about 6, 8 and 15–20 days in the second half of the time series.

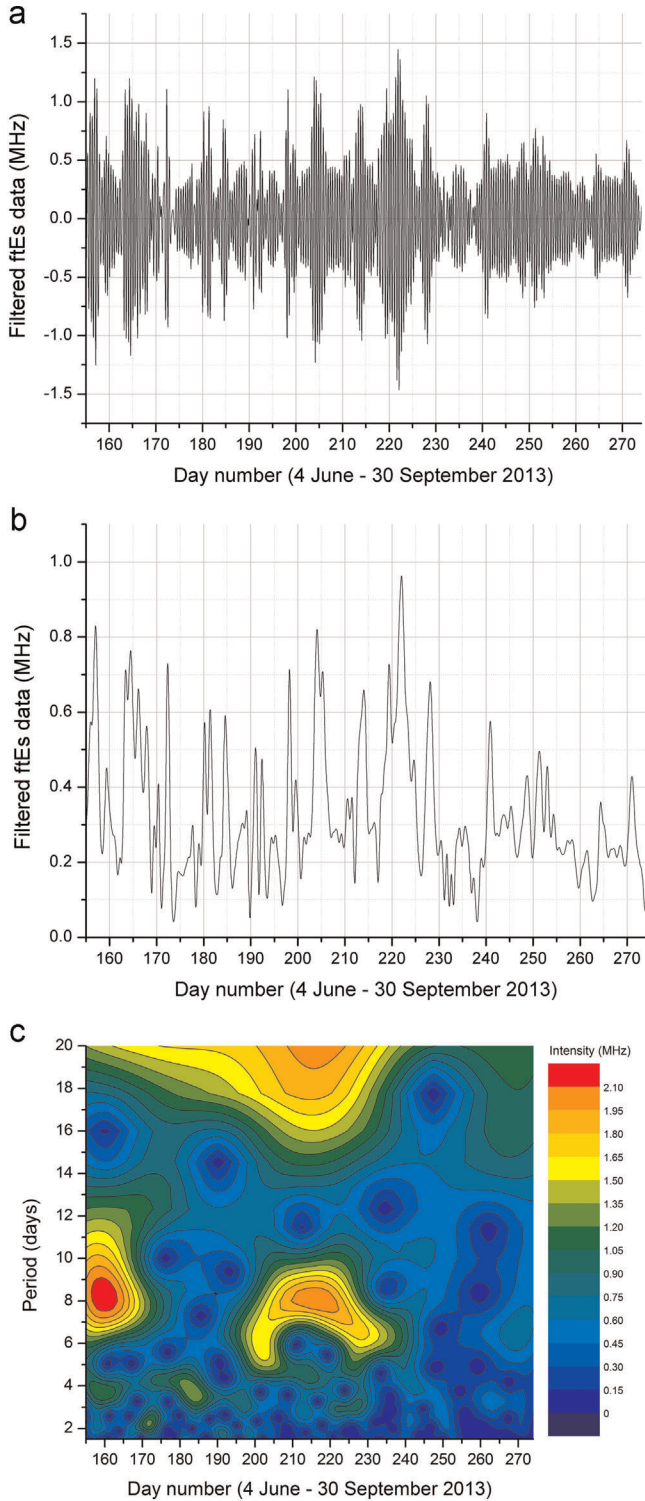


Fig. 9. (a) The ftEs signal related to the semidiurnal periodicity extracted from the spectrogram shown in Fig. 1c. (b) The ftEs semidiurnal periodicity time series obtained from the signal shown in (a) after straightening and low-filtering it. (c) The wavelet spectrogram of the time series shown in (b) for periods ranging from 1.5 to 20 days.

4.2. The case of the semidiurnal tidal periodicity

Fig. 9 is the same as Fig. 7 but related to the semidiurnal TW periodicity, that is the wavelet coefficients of Figs. 1c and 2c that have been considered in the analysis were those with periods from 10 to 14 h. Again, Fig. 9a shows that the signal appears as an AM

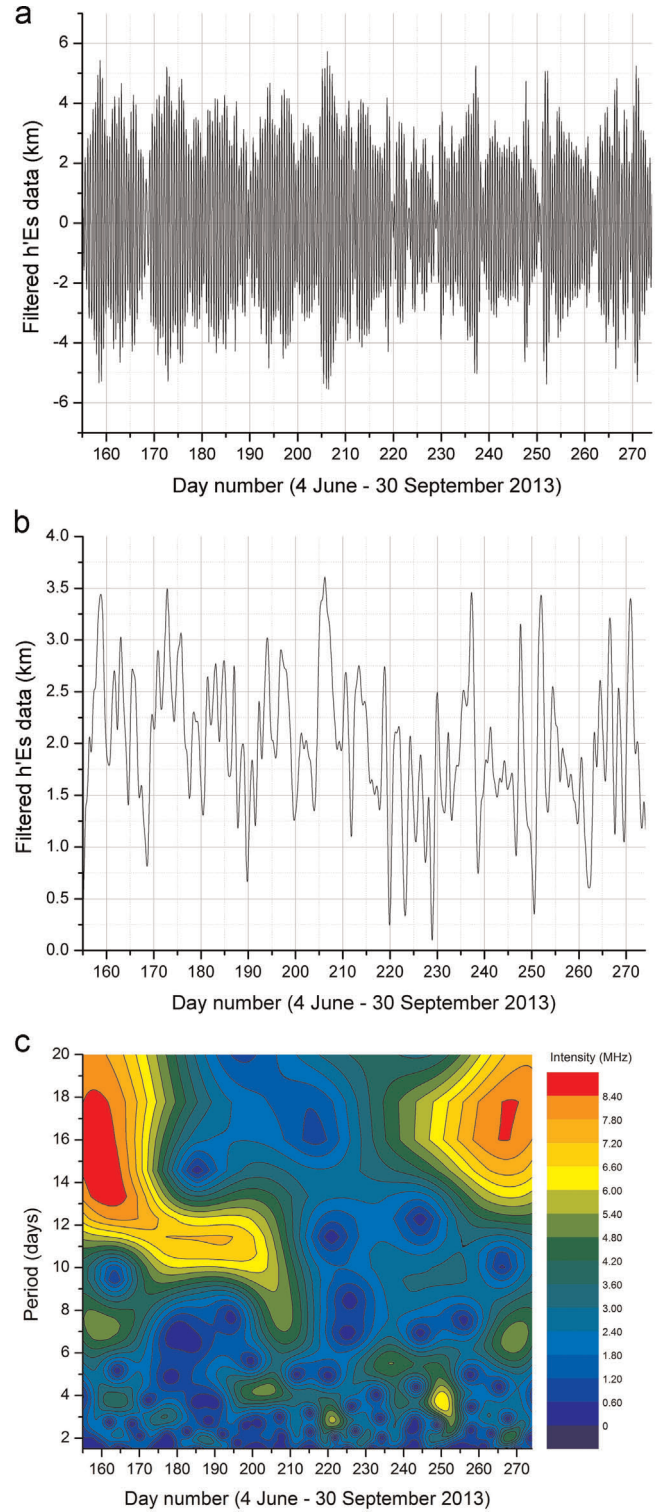


Fig. 10. (a) The h'Es signal related to the semidiurnal periodicity extracted from the spectrogram shown in Fig. 2c. (b) The h'Es semidiurnal periodicity time series obtained from the signal shown in (a) after straightening and low-filtering it. (c) The wavelet spectrogram of the time series shown in (b) for periods ranging from 1.5 to 20 days.

radio signal, it has a carrier wave with a period of 12 h and a modulating wave with a variable period of many days. Fig. 9b shows the ftEs semidiurnal periodicity time series obtained from the signal shown in Fig. 9a after straightening and low-filtering it, and Fig. 9c shows the corresponding wavelet spectrogram for the PWs periods. Fig. 9c shows that the most important feature is

associated to three large spectral peaks, the first localized between the days 155 and 170 with a period of about 8–9 days, the second between the days 200 and 235 with a period of about 8 days, the third with a period of about 20 days and more is a very large spectral peak that is present for the first half of the spectrogram.

Fig. 10 is the same as Fig. 9 but for h'Es. The wavelet spectrogram of Fig. 10c shows that the most important peaks are localized respectively in the first part of the time series with a period ranging from 13 to 18 days, and in the second part of the time series with a period centered at about 16–18 days; several small peaks with periods ranging from 2 to 8 days are also present throughout the time series.

At first glance, the results given by the wavelet spectrograms shown in Figs. 7c and 9c for ftEs, and in Figs. 8c and 10c for h'Es, present some differences, mostly the latter. Anyway, focusing the attention on the first part of the ftEs time series, specifically from the 4 June up to the 4 July 2013, Figs. 3c, 7c, and 9c present some similarities, this meaning that the wind-shear and the TW–PW nonlinear interaction theories are in agreement. This is why in the next section this ftEs time interval will be investigated in more detail.

4.3. Strong evidence of the TW–PW nonlinear interaction during the 4 June–4 July 2013 time interval

As demonstrated by Teitelbaum and Vial (1991), besides amplitude modulating the signal, the nonlinear interaction mechanism gives also rise to secondary waves causing in the spectrum the appearance of sidebands around the TW periodicities, for frequencies equal to the sum and difference of the primary wave interacting frequencies. In order to look for these secondary peaks, according to the considerations made at the end of the previous section, the ftEs data from the 4 June to the 4 July 2013 were selected, and the corresponding FFT spectra were calculated.

Fig. 11a shows the FFT amplitude spectrum of the ftEs hourly mean values of Fig. 1a falling in the considered time interval for period ranging from 2 to 36 h. This figure points out that additionally to the primary peaks due to the diurnal and semidiurnal TWs, there are secondary peaks exceeding the 95% level of confidence, the most important of which have been highlighted with arrows of different colors: the red ones at about 22 and 27 h are consistent with a nonlinear interaction between the diurnal TW and a PW with a period of about 9–10 days; the blue ones at about 19 and 31 h are consistent with a nonlinear interaction between the diurnal TW and a PW with a period of about 4–5 days; the green ones at about 11 and 13 h are consistent with a nonlinear interaction between the semidiurnal TW and a PW with a period of about 8–9 days. This preliminary results are in agreement with what is shown in Figs. 3, 7 and 9. Anyway, to deeply study this TW–PW nonlinear interaction, the FFT spectra were also calculated separately for the diurnal and semidiurnal filtered signals shown in Figs. 7a and 9a, but only for the time interval from the 4 June up to the 4 July 2013.

Fig. 11b shows the FFT amplitude spectrum of the ftEs diurnal filtered values, for periods ranging from 16 to 32 h, and points out that additionally to the primary peak due to the diurnal TW, there are secondary peaks exceeding the 95% level of confidence or close to it, the most important of which have been highlighted with arrows of different colors: the red ones at about 21.9 and 26.7 h are consistent with a nonlinear interaction between the diurnal TW and a PW with a period of about 9–10 days; the green ones at about 22.7 and 25.3 h are consistent with a nonlinear interaction between the diurnal TW and a PW with a period of about 18 days; the blue ones at about 19.4 and 31.2 h are consistent with a nonlinear interaction between the diurnal TW and a PW with a period of about 4 days. These results are in good agreement with the

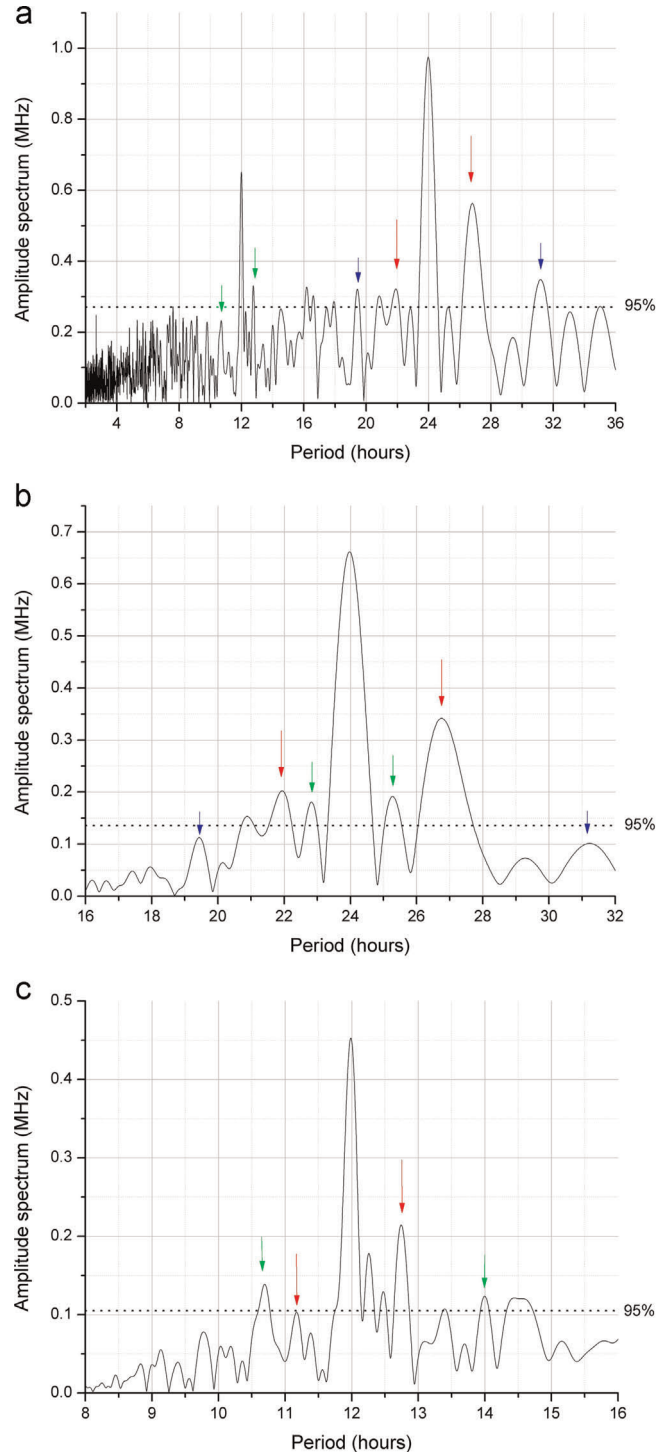


Fig. 11. (a) FFT amplitude spectrum of the ftEs hourly mean values of Fig. 1a falling in the time interval [4 June 2013, 4 July 2013], for periods ranging from 2 to 36 h. (b) FFT amplitude spectrum of the ftEs diurnal time series of Fig. 7a falling in the time interval [4 June 2013, 4 July 2013], for periods ranging from 16 to 32 h. (c) FFT amplitude spectrum of the ftEs semidiurnal time series of Fig. 9a falling in the time interval [4 June 2013, 4 July 2013], for periods ranging from 8 to 16 h. The arrows highlight the secondary peaks due to the TW–PW nonlinear interaction (see the text). The horizontal dashed lines indicate the 95% level of confidence.

wavelet spectrogram shown in Fig. 7c for the first 30 days of the time series; as expected, the most important secondary peaks are associated with the strong modulation caused by the intense peak with a period of about 9–10 days, characterizing the first part of the ftEs diurnal time series.

Fig. 11c shows the FFT amplitude spectrum of the ftEs semi-diurnal filtered values, for periods ranging from 8 to 16 h, and points out that additionally to the primary peak due to the semi-diurnal TW there are secondary peaks, the most important of which have been highlighted with arrows of different colors: the red ones at about 11.2 and 12.7 h are consistent with a nonlinear interaction between the semidiurnal TW and a PW with a period of about 8–9 days; the green ones at about 10.7 and 14.0 h are consistent with a nonlinear interaction between the semidiurnal TW and a PW with a period of about 4 days. Also these results are in good agreement with the wavelet spectrogram shown in Fig. 9c for the first 30 days of the time series; as expected, the most important secondary peaks are associated with the strong modulation caused by the intense peak with a period of about 8–9 days, characterizing the first part of the ftEs semi-diurnal time series.

5. Discussion and conclusions

Using vertical ionograms recorded during a summertime campaign (4 June–30 September 2013) by the AIS-INGV ionosondes installed at the mid-latitude ionospheric stations of Rome and Gibilmanna, Italy, the variability of the oscillations imprinted in the time series of the ftEs and h'Es characteristics that are comparable with those of the TWs and the PWs were investigated.

The main periodicities tagging both time series are at 12 and 24 h (see Figs. 1b, c and 2b, c), and this fact can be associated with the influence that semidiurnal and diurnal TWs have on the vertical wind-shear mechanism at the base of the Es formation. Actually, concerning the 24 h periodicity, it has to be taken into account also that the Es layer is characterized by a daily cycle for which the daytime layer is much stronger than the nighttime one. This is because the number of existing photo-ionized metal atoms is larger during sunlit hours, which increases the metal ion densities considerably. Hence, in reality, the strong 24 h periodicity is due to a mixing of two causes: the Es daily cycle and the tidal effect.

The ftEs time series shows values that in June and July are greater than in August and September (Fig. 1a), while the h'Es time series shows values that are nearly constant along the whole time series (Fig. 2a); this means that the ftEs characteristic strongly depends on the meteoric influx near the summer solstice as shown by Haldoupis et al. (2007), while the h'Es trend highlights that the wave activity affecting the Es layer is a phenomenon always present.

Again, Figs. 1a and 2a show that ftEs and h'Es values are amplitude modulated with periodicities of several days, and the WFT and CWT analyses (see Figs. 3a, b and 4a, b) suggest that these periodicities are likely associated with the influence of the PWs acting through their horizontal wind-shear forcing with periods close to the normal Rossby modes, that is 2, 5, 10 and 16 days (Shalimov et al., 1999; Shalimov and Haldoupis, 2002; Haldoupis and Pancheva, 2002; Pancheva et al., 2003). Anyway, concerning the main PW periods involved and their temporal localization, some differences arose between ftEs and h'Es; in fact, unlike the ftEs spectrogram (Fig. 3b), the h'Es spectrogram (Fig. 4b) shows maxima that are placed along the whole time series. At first glance, this feature would seem an unquestionable advantage for studying the influence that atmospheric waves have on Es dynamics, but this would be true if the h'Es measurements had the same resolution as ftEs. In fact, we have to take into account that the height resolution of the AIS-INGV ionosonde is 4.5 km, which is certainly constraining for studying the Es dynamics, because the thickness of the Es layer is of the order of few kilometers and then

most of Es movements occurs within the AIS-INGV height resolution.

The wavelet spectrograms of the ftEs signals related to the diurnal and semidiurnal periodicities extracted from the spectrogram shown in Fig. 1c show both similarities and differences (see Fig. 7c and Fig. 9c). In particular, both spectrograms show an important periodicity of about 8–10 days in the first part which is similar to that shown by the wavelet spectrogram of Fig. 3b related to the unfiltered time series. This suggests that, at least in the first thirty days of the measurement campaign, in the low atmosphere the PWs with such a period might have nonlinearly interacted both with the diurnal and semidiurnal TWs, and then propagated in the MLT region without suffering important changes. This fact is on the other hand confirmed also by the FFT analysis illustrated in Fig. 11 showing sidebands around the TW periodicities that, accordingly to the Teitelbaum and Vial (1991) theory, are justified in terms of the TW–PW nonlinear interaction. Anyway, other periodicities do not present the same features; for instance, the intense periodicity at 8 days in the central part of the spectrogram of Fig. 9c does not appear neither in the spectrogram of Fig. 7c nor in that of Fig. 3b. These differences can be however explained in terms of the nonlinearity of the interaction; in fact, the nonlinearity allows very intense modulations in the presence of weak interacting waves but also moderate modulations in the presence of strong interacting waves, the latter being most likely what featured the aforementioned periodicity at 8 days visible in the central part of the spectrogram of Fig. 9c. Moreover, we have to take into account that these oscillations propagate through the atmosphere, and hence it can be happened that the PW with a period of 8 days interacted with the semidiurnal TW at lower altitudes, without propagating to higher altitudes, unlike the semidiurnal TW that reaches the low ionosphere carrying with itself the modulation impressed by the PW. Moreover, it is worth reminding that the periodicities associated with the PWs are caused by the efficiency of the horizontal wind-shear mechanism, and consequently their appearance in the spectrogram could be influenced by this mechanism that could prove differently efficient for different periodicities. Anyhow, it seems that the semidiurnal and diurnal TWs can interact differently with the PWs, even though a PW much more intense than the others in all likelihood will modulate both TWs, as seen in the first part of the wavelet spectrograms of Figs. 3b, 7c, and 9c.

Unlike ftEs, the wavelet spectrograms of the h'Es signals related to the diurnal and semidiurnal periodicities extracted from the spectrogram shown in Fig. 2c show significant differences both for the corresponding intensities and for the temporal location (see Figs. 8c and 10c). For instance, the intense maximum at 11 days visible in the first part of Fig. 8c does not appear neither in Fig. 4b nor in Fig. 10c. Hence, it is difficult to claim that the semidiurnal and diurnal periodicities of h'Es are amplitude modulated by a PW simultaneously present in the ionospheric E region. At the same time, however, Fig. 2c shows that h'Es suffers an amplitude modulation. A possible explanation of this discrepancy could be related just to the nonlinearity of the TW–PW interaction and to the consequent selective propagation through the ionosphere, but the inconsistencies are so important that this explanation can be considered fully unjustified. A simpler explanation could be lie in the aforementioned low height resolution of the AIS-INGV ionosonde which is certainly not sufficient for highlighting the Es dynamics with the right accuracy by means of the h'Es characteristic, as on the contrary it is possible through the ftEs analyses. Anyway, also this explanation turns out to be unsatisfactory, because at least in part the h'Es analysis should have shown results partially concordant with those obtained by the ftEs studies. The more plausible explanation lies in the different physical meaning characterizing the two ionospheric characteristic in play. The ftEs

represents a measure of the ionic content of the Es layer, where the ions are accumulated through the wind-shear mechanism (vertical for the TWs, horizontal for the PWs), and consequently ftEs represents a measure of the efficiency of this mechanism and indirectly highlights what atmospheric wave phenomena caused the ion accumulation; for this reason, ftEs turns out to be the most suitable characteristic for studying the influence of the TWs and the PWs on Es. On the contrary, h'Es is a characteristic exclusively dynamic and hence is the most suitable one for studying the parameters associated with the TWs, but on the other hand it can reveal nothing about the efficiency of the wind-shear mechanism and consequently about the influence that the PWs have on the dynamic properties of the TWs. Hence, in the light of this, even though interesting, the h'Es results cannot be considered suitable for studying the influence of the PWs on Es, although alike ftEs it is characterized by a tidal amplitude modulation. Another important point came out from the study described in the paper is the very good correspondence between the Rome and Gibilmanna results, because this represents an evidence that the oscillations embedded in Rome and Gibilmanna data are realistic. Additionally, the distance between the two sites suggests that these oscillations are caused by large-scale processes, which is concurring with the notion of TWs and PWs. The differences characterizing in part the PW periodicities could be related to the small difference in latitude between the two sites.

Anyhow, concerning the Es dynamics complexity, it is however worth remarking that the wind-shear theory (perhaps with a small added external field) appears sufficient along with the tidal wind system to explain the mid-latitude layers that, as it has been previously said in the introduction section, are known as TILs and the features of which are somewhat consistent with the results shown in the paper. However, also at mid latitudes, there are cases of layers for which alternative formation processes are required, as electric-field-induced layers, QPE regions, and ion rains.

Finally, this study confirms that ionosonde data, especially those registered in summertime, represent a powerful tool for investigating the TW and the PW properties. In order to verify whether the features described in this paper are somehow influenced by the solar activity, it is intention of the authors to extend the analyses here illustrated also to hourly validated summertime data recorded from 1976 to 2012 at the ionospheric station of Rome.

References

- Axford, W.I., 1963. The formation and vertical movement of dense ionized layers in the ionosphere due to neutral wind shears. *J. Geophys. Res.* 68 (3), 769–779.
- Beard, A.G., Mitchell, N.J., Williams, P.J.S., Kunitake, M., 1999. Non-linear interactions between tides and planetary waves resulting in periodic tidal variability. *J. Atmos. Sol.–Terr. Phys.* 61, 363–376.
- Charney, J.G., Drazin, P.G., 1961. Propagation of planetary-scale disturbances from the lower into the upper atmosphere. *J. Geophys. Res.* 66 (1), 83–109.
- Chimonas, G., Axford, W.I., 1968. Vertical movement of temperate-zone sporadic E layers. *J. Geophys. Res.* 73 (1), 111–117.
- Dickinson, R.E., 1968. On the exact and approximate linear theory of vertically propagating planetary Rossby waves forced at a spherical lower boundary. *Mon. Weather Rev.* 96 (7), 405–415.
- Forbes, J.M., 1995. Tidal and planetary waves. In: Johnson, R.M., Killen, T.L., *The upper Mesosphere and lower Thermosphere: A Review of Experiment and Theory*, pp. 67–87.
- Fujitaka, K., Tohmatsu, T., 1973. A tidal theory of the ionospheric intermediate layer. *J. Atmos. Terr. Phys.* 35, 425–438.
- Haldoupis, C., 2012. Midlatitude sporadic E. A typical paradigm of atmosphere–ionosphere coupling. *Space Sci. Rev.* 168, 441–461. <http://dx.doi.org/10.1007/s11214-011-9786-8>.
- Haldoupis, C., 2011. A tutorial review on sporadic E layers, in *Aeronomy of the Earth's atmosphere and ionosphere*. IAGA Spec. Sopr. Book Ser. 2, 381–394. http://dx.doi.org/10.1007/978-94-007-0326-1_29.
- Haldoupis, C., Meek, C., Christakis, N., Pancheva, D., Bourdillon, A., 2006. Ionogram height-time intensity observations of descending E layers at mid-latitude. *J. Atmos. Sol.–Terr. Phys.* 68, 539–557. <http://dx.doi.org/10.1016/j.jastp.2005.03.020>.
- Haldoupis, C., Pancheva, D., Mitchell, N.J., 2004. A study of tidal and planetary wave periodicities present in midlatitude sporadic E layers. *J. Geophys. Res.* 109, A02302. <http://dx.doi.org/10.1029/2003JA010253>.
- Haldoupis, C., Pancheva, D., 2002. Planetary waves and midlatitude sporadic E layers: strong experimental evidence for a close relationship. *J. Geophys. Res.* 107 (A6), 1078. <http://dx.doi.org/10.1029/2001JA000212>.
- Haldoupis, C., Pancheva, D., Singer, W., Meek, C., MacDougall, J., 2007. An explanation for the seasonal dependence of midlatitude sporadic E layers. *J. Geophys. Res.* 112, A06315. <http://dx.doi.org/10.1029/2007JA012322>.
- Holton, J.R., 1975. *The dynamic meteorology of the stratosphere and mesosphere: Meteorological Monographs*. vol. 15. American Meteorological Society, Boston (218 pp).
- Mathews, J.D., Morton, Y.T., Zhou, Q., 1993. Observations of ion layer motions during the AIDA campaign. *J. Atmos. Terr. Phys.* 55, 447–457.
- Mathews, J.D., 1998. Sporadic E: current views and recent progress. *J. Atmos. Sol.–Terr. Phys.* 60 (4), 413–435.
- Mathews, J.D., Machuga, D.W., Zhou, Q., 2001. Evidence for electrodynamic linkages between spread-F, ion rain, the intermediate layer, and sporadic E: results from observations and simulations. *J. Atmos. Sol.–Terr. Phys.* 63, 1529–1543.
- Otsuka, Y., Onoma, F., Shiokawa, K., Ogawa, T., Yamamoto, M., Fukao, S., 2007. Simultaneous observations of nighttime medium-scale traveling ionospheric disturbances and E region field-aligned irregularities at midlatitude. *J. Geophys. Res.* 112, A06317. <http://dx.doi.org/10.1029/2005JA011548>.
- Pancheva, D., Haldoupis, C., Meek, C.E., Manson, A.H., Mitchell, N.J., 2003. Evidence of a role for modulated atmospheric tides in the dependence of sporadic E layers on planetary waves. *J. Geophys. Res.* 108 (A5), 1176. <http://dx.doi.org/10.1029/2002JA009788>.
- Pancheva, D., 2000. Evidence for nonlinear coupling of planetary waves and tides in the lower thermosphere over Bulgaria. *J. Atmos. Sol.–Terr. Phys.* 62, 115–132.
- Pancheva, D., Mukhtarov, P., Mitchell, N.J., Beard, A.G., Muller, H.G., 2000a. A comparative study of winds and tidal variability in the mesosphere/lower-thermosphere region over Bulgaria and the UK. *Ann. Geophys.* 18, 1304–1315.
- Pancheva, D., Mukhtarov, P., 2000. Wavelet analysis on transient behavior of tidal amplitude fluctuations observed by meteor radar in the lower thermosphere above Bulgaria. *Ann. Geophys.* 18, 316–331.
- Pancheva, D., Mukhtarov, P., 2011. Atmospheric tides and planetary waves: recent progress based on SABER/TIMED temperature measurements (2002–2007), in *Aeronomy of the Earth's atmosphere and ionosphere*. IAGA Spec. Sopr. Book Ser. 2, 19–56.
- Pancheva, D., Beard, A.G., Mitchell, N.J., 2000b. Nonlinear interactions between planetary waves in the mesosphere/lower-thermosphere region. *J. Geophys. Res.* 105 (A1), 157–170.
- Pezzopane, M., 2004. Interpret: a Windows software for semiautomatic scaling of ionospheric parameters from ionograms. *Comp. Geosci.* 30, 125–130. <http://dx.doi.org/10.1016/j.cageo.2003.09.009>.
- Pietrella, M., Bianchi, C., 2009. Occurrence of sporadic-E layer over the ionospheric station of Rome: analysis of data for thirty-two years. *Adv. Space Res.* 44, 72–81. <http://dx.doi.org/10.1016/j.asr.2009.03.006>.
- Rishbeth, H., Garriott, O.K., 1969. *Introduction to Ionospheric Physics*. Academic Press, New York (331 pp).
- Sauli, P., Bourdillon, A., 2008. Height and critical frequency variations of the sporadic-E layer at midlatitudes. *J. Atmos. Sol.–Terr. Phys.* 70, 1904–1910. <http://dx.doi.org/10.1016/j.jastp.2008.03.016>.
- Shalimov, S., Haldoupis, C., Voiculescu, M., Schlegel, K., 1999. Midlatitude E region plasma accumulation driven by planetary wave horizontal wind shears. *J. Geophys. Res.* 104 (A12), 207–213.
- Shalimov, S., Haldoupis, C., 2002. A model of mid-latitude E region plasma convergence inside a planetary wave cyclonic vortex. *Ann. Geophys.* 20, 1193–1201.
- Szuszczewicz, E.P., Roble, R.G., Wilkinson, P.J., Hanbaba, R., 1995. Coupling mechanism in the lower ionospheric–thermospheric system and manifestations in the formation and dynamics of intermediate and descending layers. *J. Atmos. Terr. Phys.* 57 (12), 1483–1496.
- Teitelbaum, H., Vial, F., 1991. On tidal variability induced by nonlinear interaction with planetary waves. *J. Geophys. Res.* 96 (A8), 169–178.
- Torrence, C., Compo, G.P., 1998. A practical guide to Wavelet analysis. *Bull. Am. Meteorol. Soc.* 79 (1), 61–78.
- Whitehead, J.D., 1961. The formation of the sporadic-E layer in the temperate zones. *J. Atmos. Terr. Phys.* 20, 49–58.
- Whitehead, J.D., 1989. Recent work on mid-latitude and equatorial sporadic-E. *J. Atmos. Terr. Phys.* 51 (A5), 401–424.
- Wilkinson, P.J., Szuszczewicz, E.P., Roble, R.G., 1992. Measurements and modeling of intermediate, descending, and sporadic layers in the lower ionosphere: results and implications for global-scale ionospheric–thermospheric studies. *Geophys. Res. Lett.* 19 (2), 95–98.
- Zuccheretti, E., Tutone, G., Sciacca, U., Bianchi, C., Arokiasamy, B.J., 2003. The new AIS-INGV digital ionosonde. *Ann. Geophys.* 46 (4), 647–659.